ACS Macro Letters
Letter
pubs.acs.org/macroletters

Origin of Stress Overshoot under Start-up Shear in Primitive Chain Network Simulation

Yuichi Masubuchi* and Hiroshi Watanabe

Institute for Chemical Research, Kyoto University, Gokasyo, Uji, Kyoto 611-0011, Japan

ABSTRACT: Birefringence measurement demonstrates that the segment orientation of entangled polymers overshoots on start-up of fast shear [Pearson et al. *J. Rheol.* **1989** *33*, 517−535]. The stress-optical rule holds for those polymers, so that the overshoot of orientation results in the overshoot of shear stress. On the other hand, an opposite result was deduced from the recent molecular dynamics simulation for bead−spring chain [Lu et al. *ACS Macro Lett.* **2014** *3*, 569−573]: the evolution of segment orientation does not overshoot but the chain stretch induces the stress overshoot, even at the shear rate $\dot{\gamma}$ smaller than the reciprocal Rouse time, $1/\tau_R$. In this study, we performed the primitive chain network simulation to find that our simulation reproduces the overshoot of both stress and orientation and the chain stretch exhibits a slight, monotonic increase but no overshoot. Our result is thus fully consistent with the experiment.

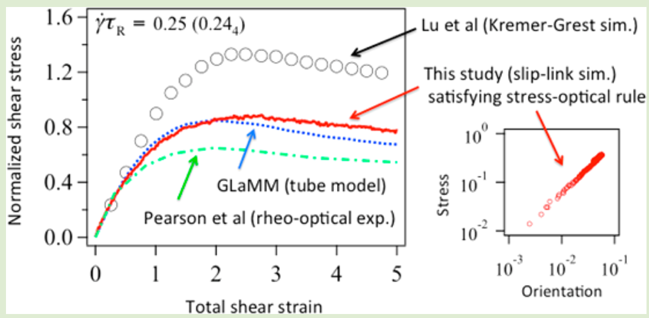

Entangled polymers exhibit the stress overshoot on start-up of fast shear. This overshoot has been related to the overshoot of the segment orientation, in particular when the flow rate $\dot{\gamma}$ is smaller than the reciprocal Rouse time $1/\tau_R$:[1] Pearson et al.[1] performed simultaneous measurements of stress and birefringence for entangled polyisoprene solutions under steady shear to find that the stress-optical rule (proportionality between the stress and birefringence) holds, even at $\dot{\gamma} > 1/\tau_R$. They also reported the birefringence growth on start-up of shear flow. Figure 1 shows their $(\Delta n/2)\sin 2\chi$ data, where Δn is the birefringence and χ is the orientation angle. (In ref 1, the data were plotted against the shearing time t. In Figure 1, t has been converted to the strain $\gamma = \dot{\gamma}t$). The Weissenberg number defined with respect to the viscoelastic Rouse relaxation time, $W_{iR}^{[G]} \equiv \dot{\gamma}\tau_R$, is 0.24_4 and 0.4_8 ($\dot{\gamma}$ = 4 and 8 s^{-1}). Clearly, the $(\Delta n/2)\sin 2\chi$ value (that corresponds to the shear stress because of the stress-optical rule) exhibits an overshoot. Similar overshoot of birefringence has been reported even earlier by Zebrowski and Fuller.[2]

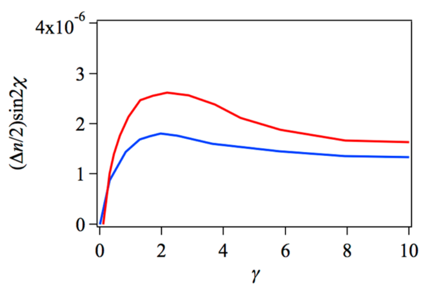

Figure 1. $(\Delta n/2)\sin 2\chi$ as a function of applied strain γ for 10% solution of polyisoprene ($M_w = 1.67 \times 10^6$, M_w/M_n = 1.1, and $M_w/M_e \sim 16.9$) dissolved in oligo-isoprene (M = 410). The $W_{iR}^{[G]}$ ($\equiv \dot{\gamma}\tau_R$) values were 0.24_4 (blue curve) and 0.48_8 (red curve), respectively ($\dot{\gamma}$ = 4 and 8 s^{-1}). The data were taken by Pearson et al.[1]

On the other hand, recently, Lu et al.[3] have reported a result contradicting to the experiment mentioned above: They performed Brownian dynamics simulations of the standard Kremer-Grest chains on start-up of shear at $1/\tau_d < \dot{\gamma} < 1/\tau_R$ (where τ_d is the longest relaxation time). The bead number per chain is 500, and the system is reasonably entangled. (Lu et al.[3] estimated the number of entanglements per chain as $500/N_e \cong 14$, with N_e = 36 being the number of beads per entanglement segment at equilibrium). The simulation showed the stress overshoot as observed in experiments, and they attempted to analyze the origin of the overshoot with respect to the chain conformation. They divided the chain into the subchains each containing the fixed number of beads, N_e = 36, and evaluated the orientation and the stretch of those subchains. Figure 2 shows the subchain orientation S^{Lu} ($=\sigma_{xy}^{or}/3G_0$ in the terminology of Lu et al.[3]) on start-up of shear at $W_{iR}^{[G]}$ = 1/12. (Lu et al.[3] defined W_{iR} with respect to the Rouse relaxation time of chain stretch and thus their W_{iR} value is twice of the viscoelastic $W_{iR}^{[G]}$ utilized in this paper.) S^{Lu} shows no overshoot and monotonically increases with increasing strain, γ, even though the stress clearly overshoots at this shear rate, $1/\tau_d < \dot{\gamma} < 1/\tau_R$.[3] Because the stretch defined in their simulation shows a clear overshoot (not shown here), Lu et al.[3] argued that the chain stretch leads to the stress overshoot. Their result, suggesting failure of the stress-optical rule even at such small $W_{iR} < 1$, is surprising since this rule is known to be valid

Received: September 28, 2014
Accepted: October 24, 2014
Published: October 27, 2014

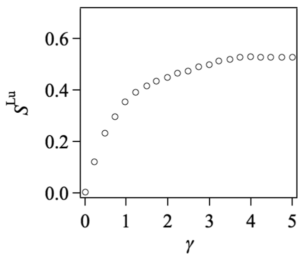

Figure 2. Subchain orientation for the bead–spring chain melt with the bead number per chain of 500 at $W_{\rm iR}^{[G]} = 1/12$. The data were reported by Lu et al.[3]

regardless of the microstructure of polymers[4] and the level of coarse-graining of molecular models.[5]

Considering the above contradiction between the experiment[1] and simulation,[3] we performed multichain slip-link simulations (primitive chain network simulations[6]) on start-up of shear. Our simulation results were consistent with the experiment by Pearson et al.[1] rather than the analysis by Lu et al.[3] Namely, the subchain orientation does overshoot to fulfill the stress-optical rule at $W_{\rm iR}^{[G]} < 1$. Details of our results are presented below.

We utilized the primitive chain network (PCN) model[6] that represents the polymer chain as consecutive subchains. Those polymer chains are bundled by slip-links to form an entangled network. Time evolution of the slip-link position obeys the Langevin-type equation of motion that considers balance of the drag force, subchain tension, osmotic force, and random force. The same force balance is also considered in the time-evolution equation for the number of Kuhn segments in each subchain to describe the sliding motion of the chain through the slip-link. The slip-link is created/removed at the chain ends, which represents constraint creation/release. The simulation based on this PCN model well reproduces the transient shear responses of entangled DNA solutions[7] and a PS melt,[8] including the stress overshoot.

In this study, we conducted the PCN simulation for the chains, each being composed of 20 subchains (entanglement segments) on average at equilibrium. Periodic boundary condition was used and the shear deformation was applied via the Lees-Edwards boundary condition and the SLLOD algorithm. The unit cell dimension was 10 × 10 × 10 (where the unit length is the average subchain length at equilibrium) and the number of chains in the box was 500. Data from 8 independent simulation runs were averaged to achieve good statistics. In this study, we did not implemented the stretch/orientation-induced reduction of friction (SORF)[8] because SORF never occurs under flow at $W_{\rm iR}^{[G]} < 1$. We also omitted the finite chain extensibility. The viscoelastic Rouse time in the PCN simulation was specified as $\tau_{\rm R} = Z_0^2\tau_0/2\pi^2$,[9] where τ_0 is the unit time in the simulation and Z_0 is the average value of the subchain number per chain.

The simulation allowed us to evaluate the evolution of shear stress σ, primitive path length L, and orientation S. The end-to-end vector of i-th subchain in j-th chain, $\mathbf{r}_{i,j} = (r_x^{i,j}, r_y^{i,j}, r_z^{i,j})$, and the number of Kuhn segments in this subchain, $n_{i,j}$, gave the shear stress as $\sigma = 3G_0^{\rm PCN}\sum_{i,j}(r_x^{i,j}, r_y^{i,j}/n_{i,j})/\sum_i Z_0$, where $G_0^{\rm PCN}$ is the unit of stress in the PCN model.[10,11] The primitive path length is straightforwardly obtained as $L = \langle \sum_i^{z_j} |\mathbf{r}_i| \rangle_j$, where Z_j is the subchain number in the j-th chain and $\langle\cdots\rangle_j$ denotes the ensemble average for all chains. The orientation is defined by $S = \langle (Z_0/Z_j)(r_x^{i,j}, r_y^{i,j}/\mathbf{r}_{i,j}^2)\rangle_{i,j}$. The factor Z_0/Z_j in this definition converts the orientation of the subchain containing $n_{i,j}$ Kuhn segments under flow ($n_{i,j}$ increases with $\dot\gamma$ due to disentanglement) into the orientation for a reference subchain containing a fixed number of Kuhn segments $n_0 = n_{\rm t}/Z_0$, where $n_{\rm t}$ is the total number of Kuhn segments per chain and n_0 is the average number of those segments per entanglement at equilibrium. The stress-optical rule is equivalent to the proportionality between the orientation S defined in this way and the shear stress, because a ratio of the optically detected segmental orientation $S^{\rm seg}$ to S of the reference subchain is constant irrespective of γ and $\dot\gamma$ given that all n_0 Kuhn segments in this subchain are mutually equilibrated in a focused time scale.[4] (This condition is always fulfilled for the entanglement segment in the PCN simulation.[9]) For comparison, we also calculated $S^{\rm ent} = \langle r_x^{i,j}\ r_y^{i,j}/\mathbf{r}_{i,j}^2\rangle_{i,j}$ for the entanglement segments under flow (subchains composed of $\langle n_{i,j}\rangle_{i,j}$ Kuhn segments on average).

Figure 3 shows the transient behavior of the reduced shear stress $\sigma/G_0^{\rm PCN}$ (top panel), the orientation S (2nd panel), and

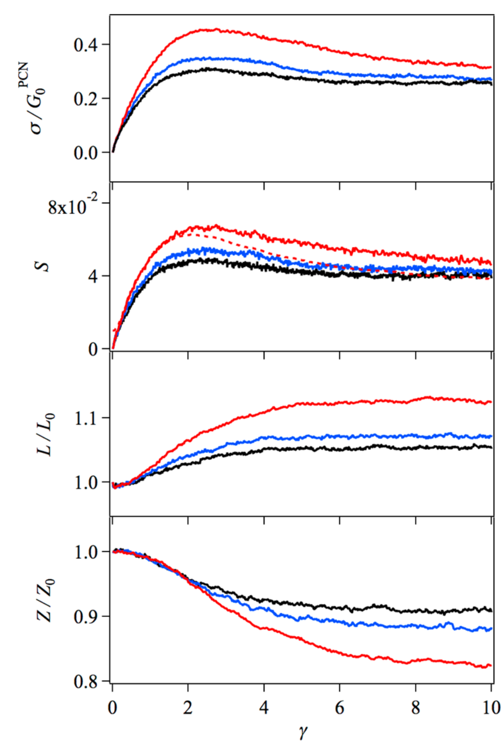

Figure 3. Reduced stress $\sigma/G_0^{\rm PCN}$, orientation S of the reference subchain (containing a fixed number n_0 of Kuhn segments irrespective of the flow condition), normalized primitive path length L/L_0, and normalized segment number per chain Z/Z_0, from top to bottom, plotted against applied strain γ ($=\dot\gamma t$). The $W_{\rm iR}^{[G]}$ values are 1/6, 1/4, and 1/2 for black, blue, and red curves, respectively. In the second panel, the dotted red curve shows $S^{\rm ent}$ of the entanglement segments (that enlarge on disentanglement).

the normalized primitive path length L/L_0 (3rd panel). (L_0 is the equilibrium value of L.) The normalized subchain number per chain Z/Z_0 is also shown (bottom panel). In the second panel, $S^{\rm ent}$ is also shown with the dotted curves. This $S^{\rm ent}$ becomes smaller than S of the reference subchain (solid red curve) at large γ (long t). This difference reflects the monotonic decay of the Z/Z_0 ratio (that is associated with the increase of L/L_0). More importantly, the overshoot is clearly noted for both $\sigma/G_0^{\rm PCN}$ and S, but not for L/L_0.

Figure 4 shows the plot of $\sigma/G_0^{\mathrm{PCN}}$ against S of the reference subchain at $W_{\mathrm{iR}}^{[G]}$ = 1/6 (black symbol), 1/4 (blue), and 1/2 (red). The proportionality between $\sigma/G_0^{\mathrm{PCN}}$ and S indicates validity of the stress-optical rule in our simulation. Note that the small stretch, characterized by the L/L_0 ratio in Figure 3, has no significant contribution to stress.

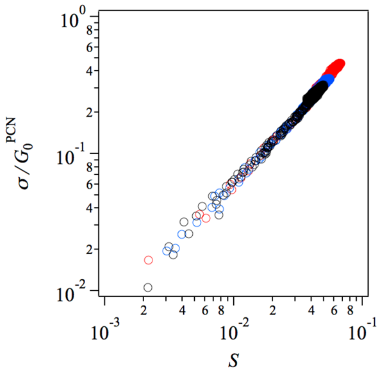

Figure 4. Shear stress $\sigma/G_0^{\mathrm{PCN}}$ plotted against orientation S. The $W_{\mathrm{iR}}^{[G]}$ values are 1/6, 1/4, and 1/2 for black, blue, and red symbols, respectively.

Figure 5 compares our results with those reported in earlier studies;[1,3,12] The viscoelastic $W_{\mathrm{iR}}^{[G]}$ is equal to 1/4 for the simulations and model calculation and is just slightly smaller for the data (green dash-dot curve; $W_{\mathrm{iR}}^{[G]} = 0.24_4$). In the top panel, the stress σ is normalized by the initial modulus G_{init}. The inset magnifies the plots for small $\gamma \leq 1$. For sufficiently small γ (short t), the linear viscoelastic behavior should prevail irrespective of nonlinearity at large γ so that the normalized σ/G_{init} should coincide with γ. In fact, this linearity requirement, $\sigma/G_{\mathrm{init}} = \gamma$ (black line in the inset), is satisfied for all cases at sufficiently small γ.

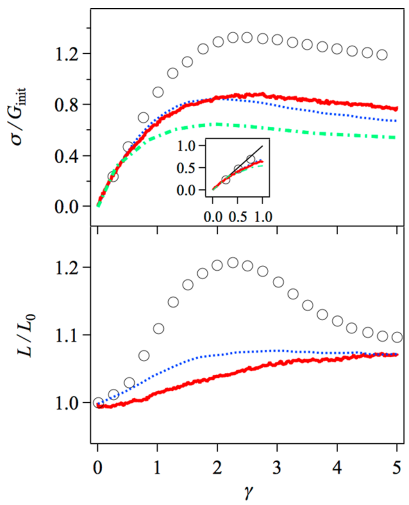

Figure 5. Reduced stress σ/G_{init} (top panel) and normalized primitive path length L/L_0 (bottom panel) plotted against applied strain γ. The inset in the top panel magnifies the σ/G_{init} vs γ plots at $\gamma \leq 1$. The data extracted from Lu et al.[3] are indicated by black unfilled circle. The result from primitive chain network simulation is drawn by red solid curve. The prediction of GLaMM model[12] (calculated by Lu et al.[3]) is presented by blue dotted curve. The stress reproduced from the birefringence reported by Pearson et al.[1] is shown by green dash-dot curve. In the inset, black line shows the slope of unity. $W_{\mathrm{iR}}^{[G]}$ is very similar for all cases; $W_{\mathrm{iR}}^{[G]}$ = 1/4 for the simulations and model calculation, and $W_{\mathrm{iR}}^{[G]} = 0.24_4$ for the experimental data.

Figure 5 demonstrates that our result (red solid curve) is rather close to the stress evolution from GLaMM model[12] (calculated by Lu et al.,[3] shown by blue dotted curve) and the rheo-optically measured stress data by Pearson et al.[1] (green dash-dot curve), in particular, at small γ, although the number of entanglement per chain was not exactly accommodated for these three cases. (The bead–spring simulation by Cao and Likhtman[13] gave similar overshoot of stress.) In contrast, the stress simulated by Lu et al.[3] (black circles) keeps the initial linear behavior up to higher strain, $\gamma \sim 0.8$, compared to the other three cases. Thus, some orientational relaxation modes appear to be suppressed in the simulation by Lu et al.,[3] as also suggested from the lack of orientation overshoot in their simulation (Figure 2). We also note that the L/L_0 ratio (Figure 5, bottom panel) obtained from our simulation and GLaMM model[12] increases monotonically with γ. This monotonic increase results from competition between the flow-induced stretch and the intrinsic (Rouse) relaxation of the chain stretch. On the other hand, in the simulation by Lu et al.[3] the L/L_0 ratio shows an overshoot.

In relation to the above results, Lu et al. recently reported (in another paper[14]) that the gyration radius $R_{g,y}$ at $W_{\mathrm{iR}}^{[G]}$ = 1/12, defined in the shear gradient direction, is considerably smaller than that at equilibrium. The PCN simulation and GLaMM model give qualitatively similar decreases of $R_{g,y}$.[15,16] This similarity may be reflected in the similarity of the steady-state value of L/L_0 for the three cases (Figure 5, bottom panel). Nevertheless, we need to accommodate the value of Z_0 to attain further assessment for the two simulations and GLaMM model. Finally, it should be also noted that the decrease of $R_{g,y}$ is not observed in rheo-dielectric experiments[16,17] (that detects the end-to-end fluctuation in the shear gradient direction). Thus, the simulations/model need to be refined for this point.

In summary, we performed the PCN simulation on start-up of shear flow to discuss the origin of the stress overshoot of entangled polymers. Following the recent study by Lu et al.,[3] the shear rates were set to be smaller than the reciprocal of the viscoelastic Rouse time. The orientation and the stress obtained from our PCN simulation commonly exhibited the overshoot and satisfied the stress-optical rule. On the other hand, the stretch slightly and monotonically increases with strain without showing the overshoot. We thus concluded that the stress overshoot is attributable to the overshoot in orientation. These results are fully consistent with the experimental result reported by Pearson et al.[1]

■ AUTHOR INFORMATION

Corresponding Author

*E-mail: mas@scl.kyoto-u.ac.jp. Tel.: +81-774-38-3136. Fax: +81-774-38-3139.

Notes

The authors declare no competing financial interest.

■ ACKNOWLEDGMENTS

Y.M. is financially supported by Grant-in-Aid for Scientific Research (B) No. 26288059 from JSPS.

■ REFERENCES

(1) Pearson, D. S.; Kiss, A. D.; Fetters, L. J.; Doi, M. *J. Rheol.* **1989**, *33*, 517–535.

(2) Zebrowski, B. E.; Fuller, G. G. *J. Polym. Sci., Polym. Phys. Ed.* **1985**, *23*, 575–589.
(3) Lu, Y.; An, L.; Wang, S.; Wang, Z. *ACS Macro Lett.* **2014**, *3*, 569–573.
(4) Janeschitz-Kriegl, H. *Adv. Polym. Sci.* **1969**, *6/2*, 170–318.
(5) Watanabe, H. *Prog. Polym. Sci.* **1999**, *24*, 1253–1403.
(6) Masubuchi, Y.; Takimoto, J.; Koyama, K.; Ianniruberto, G.; Marrucci, G.; Greco, F. *J. Chem. Phys.* **2001**, *115*, 4387–4394.
(7) Masubuchi, Y.; Furuichi, K.; Horio, K.; Uneyama, T.; Watanabe, H.; Ianniruberto, G.; Greco, F.; Marrucci, G. *J. Chem. Phys.* **2009**, *131*, 114906.
(8) Yaoita, T.; Isaki, T.; Masubuchi, Y.; Watanabe, H.; Ianniruberto, G.; Marrucci, G. *Macromolecules* **2012**, *45*, 2773–2782.
(9) Furuichi, K.; Nonomura, C.; Masubuchi, Y.; Watanabe, H.; Ianniruberto, G.; Greco, F.; Marrucci, G. *Rheol. Acta* **2008**, *47*, 591–599.
(10) Masubuchi, Y.; Ianniruberto, G.; Greco, F.; Marrucci, G. *J. Chem. Phys.* **2003**, *119*, 6925–6930.
(11) Masubuchi, Y.; Ianniruberto, G.; Greco, F.; Marrucci, G. *J. Non-Newtonian Fluid Mech.* **2008**, *149*, 87–92.
(12) Graham, R. S.; Likhtman, A. E.; McLeish, T. C. B.; Milner, S. T. *J. Rheol.* **2003**, *47*, 1171–1200.
(13) Cao, J.; Likhtman, A. E. *Phys. Rev. Lett.* **2012**, *108*, 028302.
(14) Lu, Y.; An, L.; Wang, S.-Q.; Wang, Z. *Macromolecules* **2014**, *47*, 5432–5435.
(15) Uneyama, T.; Masubuchi, Y.; Horio, K.; Matsumiya, Y.; Watanabe, H.; Pathak, J.; Roland, C. *J. Polym. Sci., Part B: Polym. Phys.* **2009**, *47*, 1039–1057.
(16) Horio, K.; Uneyama, T.; Matsumiya, Y.; Masubuchi, Y.; Watanabe, H. *Macromolecules* **2014**, *47*, 246–255.
(17) Watanabe, H.; Ishida, S.; Matsumiya, Y. *Macromolecules* **2002**, *35*, 8802–8818.

dx.doi.org/10.1021/mz500627r | *ACS Macro Lett.* 2014, 3, 1183–1186